SOFT ROBOTICS
Volume 00, Number 00, 2017

DOI: 10.1089/soro.2016.0052

SoRo
Soft Robotics

ORIGINAL ARTICLE

Modeling and Experimental Evaluation of Bending Behavior of Soft Pneumatic Actuators Made of Discrete Actuation Chambers

Gursel Alici,[1,2] Taylor Canty,[1] Rahim Mutlu,[1,2] Weiping Hu,[1] and Vitor Sencadas[1,2]

Abstract

In this article, we have established an analytical model to estimate the quasi-static bending displacement (i.e., angle) of the pneumatic actuators made of two different elastomeric silicones (Elastosil M4601 with a bulk modulus of elasticity of 262 kPa and Translucent Soft silicone with a bulk modulus of elasticity of 48 kPa—both experimentally determined) and of discrete chambers, partially separated from each other with a gap in between the chambers to increase the magnitude of their bending angle. The numerical bending angle results from the proposed gray-box model, and the corresponding experimental results match well that the model is accurate enough to predict the bending behavior of this class of pneumatic soft actuators. Further, by using the experimental bending angle results and blocking force results, the effective modulus of elasticity of the actuators is estimated from a blocking force model. The numerical and experimental results presented show that the bending angle and blocking force models are valid for this class of pneumatic actuators. Another contribution of this study is to incorporate a bistable flexible thin metal typified by a tape measure into the topology of the actuators to prevent the deflection of the actuators under their own weight when operating in the vertical plane.

Keywords: soft pneumatic actuators, mathematical modeling, soft robotic gripper, soft robotics

Introduction

As an emerging field of robotics, soft robotics is the science and engineering of the robots that are primarily made of soft materials, components, and active structures such that they can safely interact and adapt with the natural world better than their predecessors (i.e., robots made of hard components).[1–4] Soft robots can be made of a number of rigid components or links that are connected to each other with single degree-of-freedom joints, such as hyper-redundant manipulators or robots, whose each joint is controlled independently to realize a task or purpose.[4–7] However, this approach requires sophisticated algorithms to control not only the position of each link/component and whole robot but also any interaction or contact between the robot and its physical environment. In line with recent progress in soft smart materials and additive manufacturing techniques, soft robots are expected to consist of a monolithic (i.e., continuum) structure containing actuation, sensing, motion/force transmission mechanism, and energy storage (including batteries) units with a minimum footprint to minimize the demand on sensory feedback and control. Such soft robots are expected to change their effective stiffness to provide a desired force when operating in various environments and interacting with various objects. When there is an application where a safe human-machine interaction and adaptability with the physical environment are required, there will be a need for a soft robotic system with variable and programmable stiffness.

Another feature of soft robots is to incorporate the concept of morphological computation into their design.[8,9] The aim is to use the topology/morphology of the robot or its materials or its interaction with the environment, or a combination of these to minimize the efficacy or function required from the controller. In short, the control functions are distributed over the morphology, materials, and constraints associated with a robot-environment interface. A typical example to morphological computation is to employ the concept of under-actuation to activate a multi-fingered gripper or a prosthetic hand.[10]

[1]School of Mechanical, Materials, Mechatronic and Biomedical Engineering, University of Wollongong, Wollongong, Australia.
[2]ARC Center of Excellence for Electromaterials Science, University of Wollongong, Wollongong, Australia.

Actuation is the most important feature to address when establishing soft robotic systems.[1,2,11–18] Pneumatic and hydraulic actuators are favorable actuators to provide a high power density.[18–26] Soft pneumatic actuators have a high power density, are lightweight, low cost, and provide the advantages of soft contact with a better morphing ability. They are also easy to manufacture by using additive manufacturing and molding techniques, which is why they have recently been the actuators of interest for soft robotic systems. Therefore, significant research efforts have been dedicated to establishing soft robotic fingers or hands or systems articulated with pneumatic actuators.[11–16,19,20] The idea of using pneumatic networks consisting of small channels embedded in a slender body made of a hyper-elastic material such as silicone was reported by Wakimoto *et al.*[11] and Mosadegh *et al.*[13] The channels can strategically be placed in a continuum body or in a discrete manner with gaps in between their exterior walls, removing the constraining effect of the continuum body, allowing large amplitude bending under the same input pressure. Former topology is named as slow pneumatic actuators, whereas the latter is named as faster actuators,[13] due to the nonconstraining chambers. The former will require much higher pressures than the latter to generate the same bending displacements. The chambers are designed in such a way that they allow a fast expansion in the longitudinal direction, with no discernible deformation in other directions, allowing a large bending of the slender body like a one-end fixed beam and the other like an end-free cantilever beam.

The performance of these actuators has been quantified experimentally and empirically by using finite element modeling and analysis. For example, Wakimoto *et al.*[11] reported on the analysis, fabrication, and performance characterization of silicone rubber, discrete chamber actuators. The finite-element method is used to undertake the analysis and optimization of these actuators. Polygerinos *et al.*[12] have reported the establishment of quasi-static analytical and finite element models for fiber-reinforced pneumatic bending actuators made of hyper-elastic silicones, not for chamber-based pneumatic actuators considered in this study. Hwang *et al.*[25] proposed pneumatic actuators consisting of trapezoidal vertical microballoon fins that were fabricated by using 3D fabricated molds. The performance of the actuators and their use in multi-finger grippers are comprehensively presented.

Recently, Yap *et al.*[26] reported on employing a low-cost printer based on fused deposition modeling (similar to the one used in this study to fabricate the molds) by using a soft commercial material called Ninjaflex (Shore Hardness 85A) to fabricate soft actuators with pneumatic chambers, which were previously fabricated by using silicone-based materials such as Ecoflex 030 and molding techniques.[11,13] This direct fabrication does not require supporting material, whose removal is a time-consuming process, to construct the actuation chambers or networks. The primary issues associated with these actuators are that their durability is low, they require high actuation pressures, and their stiffness is constant. The high pressure and durability are coupled; the lower is the pressure, the higher is the durability. But the lower is the pressure, the lower is the bending angle or displacement output and force output. Recently, Agarwal *et al.*[27] have proposed a new soft pneumatic actuator concept based on shell-reinforced patterns made of polyethylene terephthalate (PET) and a single air chamber made of a highly elastomeric material to allow bending and linear motions. The unstretchable shell enclosing the actuator chamber facilitates either bending motion or linear extension motion, depending on the pattern of the shell. Finite element analysis has been used to optimize the design parameters, and to predict the performance and behavior of the actuators. Although they have employed the Ogden model to represent the nonlinear behavior of the air chamber in the actuators, the linear elastic model is used to represent deformation of the shell.

There has been limited progress on establishing analytical models to better explain the phenomenon behind actuation and, more importantly, to use these models to better predict quasi-static and dynamic behavior of the chamber-based actuators. With this in mind, we propose an effective analytical bending angle model and its experimental validation for this class of actuators. We also present a fabrication technique that requires fewer steps than the fabrication techniques reported earlier for the same type of actuators.[11–13,28,29] Another contribution of this study is to propose a bistable flexible thin metal typified by a tape measure to prevent deflection of the actuator under its own weight when operating in the vertical plan. This is a simple and effective way to keep the actuators in their straight configuration under no input. As the slender pneumatic actuators have a composite structure and nonlinear properties of the elastomeric materials are used to construct the actuator, it is not straightforward to experimentally determine their modulus of elasticity by using the classical technique of tensile tests. We have experimentally measured the bending angle versus pressure, and blocking force versus pressure data to identify the effective modulus of the actuators made of Elastosil M4601 with a bulk modulus of elasticity of 262 kPa and a relatively Soft Translucent silicone with a bulk modulus of elasticity of 48 kPa. We fabricated two actuators made of the same silicone: one with a constraining paper layer, and one with a bistable and flexible thin metal. In total, four actuators have been experimented with to validate the analytical bending angle model.

In the Description and Fabrication of Soft Pneumatic Actuators section, we describe the soft pneumatic actuators and their fabrication, and we experimentally determine the moduli of elasticity of the silicones that they are fabricated from. The Derivation of Bending Angle Model section covers the derivation of the gray-box bending angle model, blocking force model, and a simple kinematic model. The experimental results and validation of the models are presented in the Experimental Validation of Analytical Models section. The application of the proposed actuator to establish a soft robotic gripper consisting of three fingers and the use of the gripper in handling a regular object and an irregular object are discussed in Applicability: A Soft Robotic Gripper section. Conclusions and future work are presented in the Conclusions and Future Work section.

Description and Fabrication of Soft Pneumatic Actuators

The soft pneumatic actuator considered in this study is shown in Figure 1. It has a slender structure populated with discrete pneumatic chambers that are also known as pneumatic networks.[11–15] Each chamber is separated into two subchambers by a rigid rib, which simplifies its fabrication

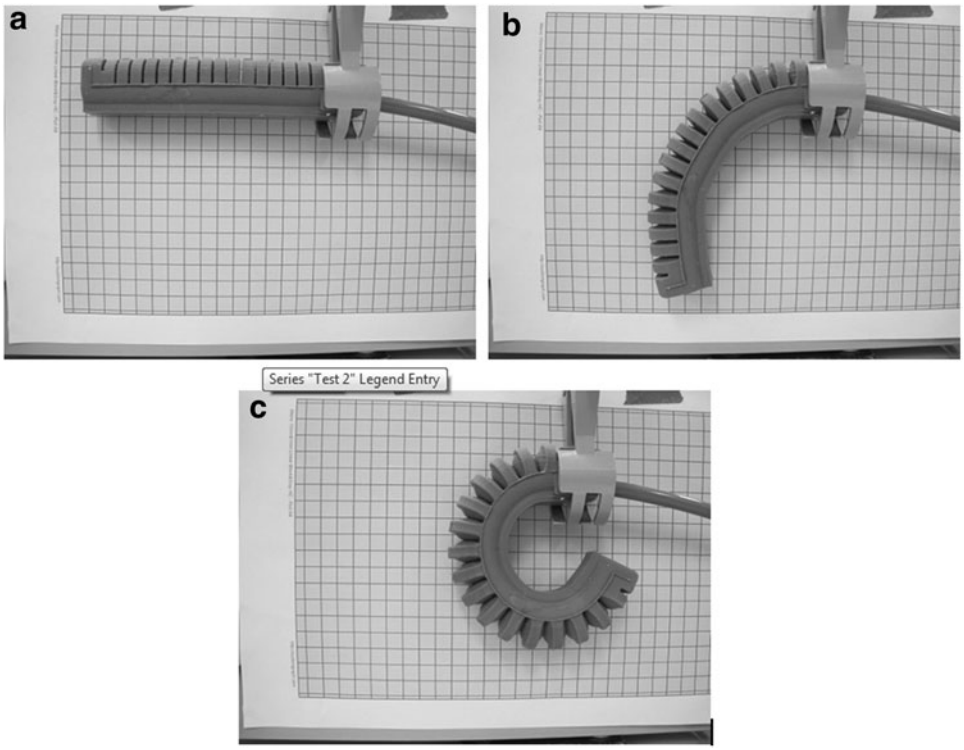

FIG. 1. Configurations of the soft pneumatic actuator under various pressures: **(a)** $P = 0$ kPa, **(b)** $P = 60$ kPa, and **(c)** $P = 100$ kPa.

compared with the fabrication of the previously published chamber-based pneumatic actuators based on molding techniques. Another advantage of the ribs is that they prevent the expansion in the transverse directions. The chambers expand in the longitudinal direction of the actuator when activated pneumatically. Although this is one way of adding structural strength to the actuator and preventing transverse deflection, the same constraining effect can be obtained by using fiber windings or shells as well reported in the literature.[12,13,20,21,27]

As shown in Figure 1, the cantilevered actuator turns into a circular shape under a constant gauge pressure of P. Its tip point generates deflections in the longitudinal and transverse directions, as shown in Figure 2. These deflections cannot be estimated by using the classical beam theory, which is as accurate as 5% for the transverse beam deflections less than 20–30% of the beam length and assumes a negligibly small longitudinal deflection.[30] The soft pneumatic actuators made of hyper-elastic materials generate large deflections, which introduce geometric nonlinearities and the material nonlinearities in their mechanical output.[20–24,27,31] Therefore, there is a need for an effective mathematical model to estimate the bending displacements or the bending angle of the soft cantilevered actuator as a function of the input pressure.[11–17,32,33] Further, this model can be used to experimentally estimate the nonlinear parameters of the actuators such as an effective modulus of elasticity.

Fabrication of actuators

The actuator was fabricated by using either of the two types of elastomeric silicones (Elastosil M4601, Barnes, and Soft Translucent, Dalchem), and it was embedded with either a bistable layer (a thin flexible metal typified by a tape measure) or an inextensible layer (paper). In total, we fabricated and tested four actuators in this study. The actuators made of Elastosil M4601 and Soft Translucent silicone are simply called A1 and A2, respectively, for the sake of brevity in the rest of the article. We used a low-cost 3D printer to manufacture the mold that comprised three components.

The fabrication process is designed so that an actuator can be molded in one stage. This is an advantage over the similar actuators that are fabricated by using a two-stage process to create the chambers first and then to close the chambers with a separately prepared layer, obtaining a nonextensible layer such as a piece of paper or a piece of cloth or fibrous layer.[13–16,34]

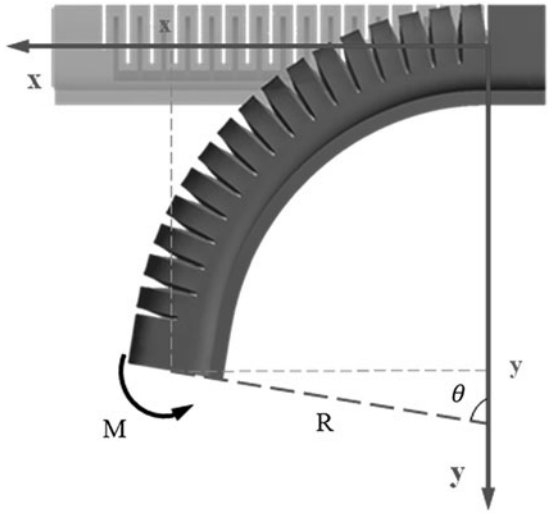

FIG. 2. Deflection of a flexible beam (corresponding to the pneumatic actuators considered in this study) under an external moment M acting at its tip, resulting in a circular configuration.

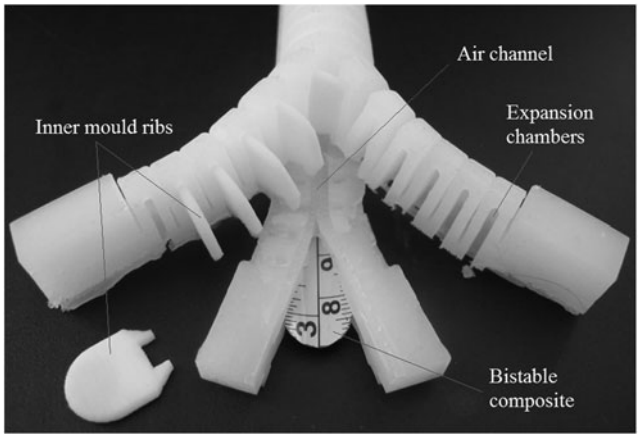

FIG. 3. Dissection of the actuator made of translucent silicone with a bistable component that is a strip of a tape measure.

As a first step, the inner mold was placed onto the lower mold with the spine jig in place. This step is to ensure the inner and outer molds are oriented correctly. The silicone was combined with its polymerization agent at a 9:1 and 10:1 weight ratio for the Elastosil M4601 and Soft Translucent silicones, respectively. The liquid silicone was thoroughly stirred so as not to fold air into the mixture. The mixture was then left to sit for ~5–10 min to let some of the bubbles rise out. The liquid silicone was then poured into the assembled mold chambers in a long, thin stream to help prevent build-ups of air bubbles. The chambers of the outer mould were filled with just enough silicone such that it touched or engulfed the inner mold.

Using a vacuum desiccator, the mold and its contents were de-gassed. This expanded the mixture and caused most of the air bubbles to precipitate out. The silicone mold was cured in a chemical oven at 70°C for ~20–25 min. The upper mold was then clicked into the lower mold. The liquid silicone was then poured into the mold to just below the top of the upper mold, ensuring ~4–5 mm of space was left for the constraining material that was either a tape measure or a piece of paper. The mold and its contents were de-gassed and cured in the chemical oven at 70°C for another 20–25 min. The bistable material (illustrated in Fig. 3) or inextensible material was cut to size and placed inside the top of the mold. The remainder of the liquid silicone was then poured into the assembled mold, filling it to the top. Care was taken to ensure that air was not trapped underneath the constraining material as this would affect its behavior. Once more, the mold and its contents were de-gassed and then cured in the oven at 70°C for another 20–25 min.

The actuator was then removed from the mold assembly. The ribs were then snapped away from the inner mold by bending the chambers, with care taken to ensure that all ribs were separated from the inner mold. Finally, the spine of the inner mold was removed by using pliers, leaving the ribs in the chambers, as shown in Figure 3.

Soft robots are inherently soft in composition; however, they are expected to perform tasks that are analogous to those of rigid robots and, thus, must, in some ways, behave rigidly. This issue was obvious during the design stage where the actuator would, at zero input pressure, bend under its own weight. Had the weight of the actuators been minimized such that there was negligible bending at zero pressure, there was still a fundamental lack of rigidity that would allow this actuator to be used in any practical scenario. To increase the actuator's rigidity by slightly increasing the input pressure, we propose an embedded bistable flexible thin metal in the form of a tape measure. Actuators embedded with an inextensible material such as a piece of paper, as suggested by Mosadegh *et al.*,[13] are restricted in one plane, turning any extension force into a bending moment. They are, however, still inherently prone to bending under their own weight and do not have sufficient rigidity such as that of the human spine or fingers.

By embedding the actuator with a bistable material such as a strip of tape measure as pictured in Figure 3, the actuator would behave stiff under zero input conditions and at a reasonably small input pressure would ''kick'' into its second state of mechanical stability, allowing bending. Such a material would also be inextensible, preventing lateral extension, analogous to the fibrous layer, simultaneously undertaking two functions.[11–14,20,21]

Determination of modulus of elasticity

The elastic modulus of the Elastosil M4601 and the Soft Translucent silicones, prepared like described in the Fabrication of Actuators section, was determined by using tensile tests (Instron tensile machine). Five samples were produced for each elastomer to find the average modulus of elasticity. The test pieces were manufactured by using a dog-bone

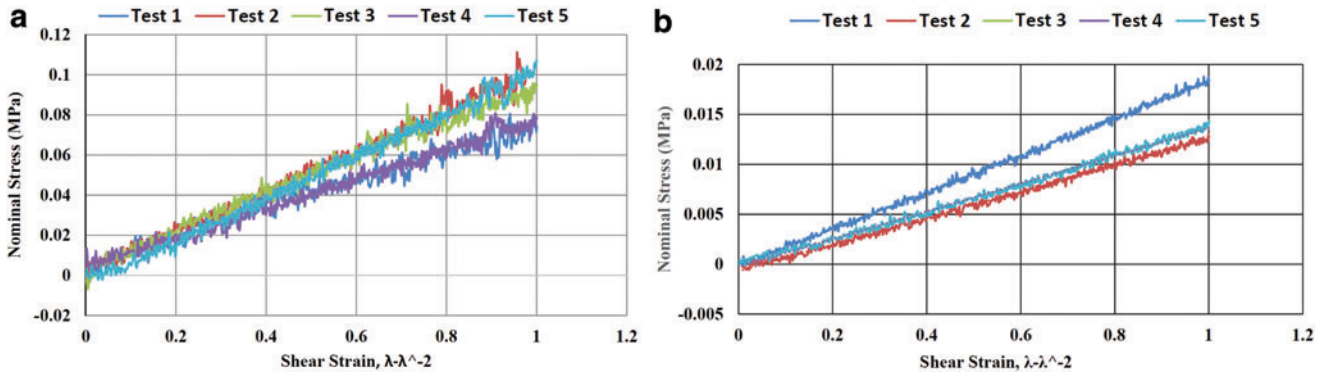

FIG. 4. Nominal stress versus shear strain data (from five tests) to estimate the elastic modulus for **(a)** Elastosil silicone rubber (*top*), and **(b)** for Soft Translucent silicone (*bottom*). Color images available online at www.liebertpub.com/soro

Table 1. Modulus of Elasticity Results for Both Silicones from the Tensile Tests

Tests	*Elastic modulus E at 100% shear strain, Elastosil M4601 silicone, kPa*	*Elastic modulus E at 100% shear strain, Soft Translucent silicone, kPa*
1	203.1	61.5
2	299.1	39.6
3	271.8	41.7
4	221.7	55.5
5	316.2	41.7
Average	262.4 ± 48.7	48.0 ± 9.9

stencil cutter with the dimensions of 10 mm in length, 2 mm in width. The thicknesses of Elastosil silicone and Soft Translucent silicone were 115 and 900 μm, respectively. For hyper-elastic materials, the modulus of elasticity is not constant as the stress-strain relationship is nonlinear. This is because the cross-links between the polymer chains undergo realignment when induced with a strain. Once all the cross-links have aligned with their respective polymer chains, the sample should fail shortly thereafter. Therefore, we have used the relationship between nominal stress σ_n, the shear strain between the polymer chains, and the shear modulus of elasticity, which is given by[35]

$$\sigma_n = G\left(\lambda - \lambda^{-2}\right) \tag{1}$$

where λ is the extension ratio given by $\lambda = 1 + \varepsilon$, and ε is the strain. The modulus of elasticity E for elastomers with a large-strain elasticity is E = 3G. It must be noted that Equation (1) is valid under the following assumptions: (1) The silicones are isotropic in all directions, and (2) they are incompressible.[35] The experimental results from both silicones and the corresponding average modulus of elasticity from these tests are shown in Figure 4 and Table 1, respectively.

Derivation of Bending Angle Model

The material used to make A1 and A2 is an elastomeric material with a nonlinear stress-strain curve. Further, the deflection of the actuators is nonlinear, which cannot be estimated by using the classical beam theory. This follows that there are two sources of nonlinearities (material and geometric nonlinearity). The material nonlinearity is especially significant under compression stresses, as reported in Refs.[11,13] In this article, we assume that the material is under a tensile stress, which has a linear relationship with the resulting strain for strains up to 70% (Figure 3 of Ref.[12]). When the actuators are in action, they are in the form of a cantilevered beam. Using Euler–Bernoulli principle,[30,36] the radius of curvature of the actuator configuration in Figure 2 is given by

$$\frac{1}{\mathrm{R}} = \frac{M}{\mathrm{EI}} \tag{2}$$

where R, E, and I are the radius of the curvature, modulus of elasticity, and area moment of inertia of the deflected beam or actuator, respectively. Assuming (as illustrated in Fig. 1) that it bends into a constant curvature shape, the corresponding bending angle θ is simply

$$\theta = \frac{L}{\mathrm{R}} \tag{3}$$

When the pressure P is applied to the actuator through the chambers distributed along the actuator length, it will apply a tensile force on the inner surface of the chamber, given by

$$F = P\,A \tag{4}$$

If the cross-sectional area of the chamber is regular like a circle or a sphere or a rectangle, the neutral axis will pass through the center of pressure, and the actuator will expand uniformly in all directions, with no bending. On the other hand, if there is a slight offset between the center of pressure and the neutral axis of the actuator, the actuator will bend toward the side where the neutral axis is. The moment causing this bending is simply the tensile force F multiplied by the offset "e" between the center of pressure and the neutral axis, as shown in Figure 5a. The tensile force and the corresponding bending moment act on the cross-section at the neutral axis, as illustrated in Figure 5a. The force acting on this cross-section is equal to the tensile force acting on the inner surface of the chamber:

$$P\,A = \sigma_t A_w \Rightarrow\ \sigma_t = P\frac{A}{A_w} \tag{5}$$

This stress σ_t should be less than the tensile strength of the materials (which is 6.5 MPa for Elastosil M4601) from which the chambers are fabricated.

Under the tensile force F (Fig. 5a), the length of the chamber or the actuator segment will change by δL_i, which is given by

$$\delta L_i = \frac{FL_i}{A_w E} = \frac{PAL_i}{A_w E} \tag{6}$$

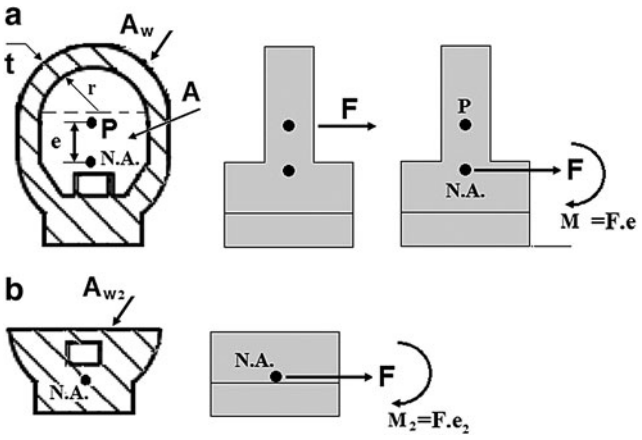

FIG. 5. **(a)** Cross-section of each chamber and the resulting geometry under an internal pressure of P, the force F acting [Eq. (4)] at the center of the chamber, and this force is transferred to the neutral axis of the cross-section with a bending moment M, and **(b)** cross-section outside or between two chambers. It must be noted that the area of this cross-section A_{w2} is much smaller than the cross-section A_w in **(a)** and is further from the center of pressure, allowing more bending of the actuator.

Table 2. Experimental Data Used to Estimate the Flexural Rigidity for A1

				Actuator 1: Elastosil, M4601						
Pressure, kPa	0	10	20	30	40	50	60	70	80	90
Angle, degree	0	15.4751	33.6811	56.4385	79.196	106.505	129.2625	165.6744	192.9834	206.6379
Force, N	0	0.133	0.2866	0.4506	0.6116	0.7728	0.9663	1.1717	1.4012	1.6767

Similarly, under the bending moment (Fig. 5a) $M = P\ A\ e$, the radius of curvature is given by

$$\frac{1}{\mathrm{R}} = \frac{P\ A\ e}{\mathrm{EI}} \tag{7}$$

When the actuator bends to a steady-state configuration like in Figures 1 or 2, the new length of the actuator is

$$\mathrm{L} = \mathrm{L}_i + \delta \mathrm{L}_i \tag{8}$$

Substituting Equations (6)–(8) into Equation (3) results in an analytical expression for the steady-state bending angle of the actuator:

$$\theta(P) = \frac{P\ A\ e}{EI}(L_i + \delta L) = \frac{P\ A\ e}{EI}\left(L_i + \frac{PAL_i}{A_w E}\right) = \underbrace{\frac{L_i\ A^2\ e}{A_w E^2 I}}_{C} P^2 + \underbrace{\frac{L_i\ A\ e}{EI}}_{D} P = CP^2 + DP \tag{9}$$

This follows that the bending angle is a nonlinear function of the bending pressure, assuming that the other parameters in Equation (9) do not change with the bending of the actuator. It must be noted that the second-order term (P^2) is inversely proportional to the square of the modulus of elasticity E. For an actuator made of a relatively stiff material, this term can be disregarded and the actuator will show a linear bending angle versus pressure behavior. It must be noted that this model considers the chamber and gap between two chambers as a single unit with a length of L_i.

We have derived Equation (9), by assuming that (1) the actuator cross-sections are perpendicular to the neutral axis during the deformation or bending, (2) any deformation of in the chambers and cross-sections in the transverse directions are negligibly small, and the modulus of elasticity of the actuator is constant.

It must be noted that this analytical model in Equation (9) can be extended to the slender actuators with no external gaps between the chambers—the actuator is a slender soft structure with an offset between its center of pressure and the neutral axis. When there is a gap or space between the external walls of two consecutive chambers, there will be two cross-sectional areas bearing the bending moment M and axial force F as shown in Figure 5a, b, respectively. With this in mind, the total angular deflection of the actuator, which is the sum of the deflections in these two cross-sections, is obtained by applying Equation (9) to two cross-sectional areas of A_w and A_{w2}. When the gap between the chambers is widened, the length of the cross-section A_{w2} increases, which results in a higher strain in this cross-section and, subsequently, a larger overall angular deflection, as presented in the Experimental Validation of Analytical Models section.

Blocking force model

We drive an analytical force model based on the volume change in the chambers under a constant pressure. When a constant gauge pressure P is applied to the actuator, the chambers primarily expand in the longitudinal direction, forming a convex shape, as shown in the actuator in the bottom image of Figure 1. For a volume change dV in the actuator under the pressure P, the input work dW_{in} causing the bending of the actuator is:

$$dW_{in} = P\ dV \tag{10}$$

For a cantilevered actuator free to bend under the pressure, the work output dW_{out} can be related to the resultant bending moment M acting at the tip of the actuator and the corresponding bending angle $d\theta$;

$$dW_{out} = M\ d\theta \tag{11}$$

When the actuator is in the blocked force configuration, the bending moment is equal to the blocked F_B times the length L of the actuator. Using the definition of mechanical efficiency η, the work output is given by

$$\mathrm{dW}_{out} = \eta\ \mathrm{dW}_{in} \tag{12}$$

Substituting Equations (10) and (11) into Equation (12) results in

$$F_B L\ d\theta = \eta\ P\ dV \Rightarrow\ F_B = \eta \frac{dV}{d\theta}\left(\frac{P}{L}\right) \tag{13}$$

Equation (13) can be written in terms of the volume change and bending angle change per unit time as

Table 3. Experimental Data Used to Estimate the Flexural Rigidity for A2

				Actuator 2: Translucent silicone			
Pressure, kPa	0	5	10	15	20	25	30
Angle, degree	0	13.6545	50.0664	91.0299	127.4419	154.7508	182.0598
Force, N	0	0.0795	0.1341	0.2339	0.3087	0.3926	0.5543

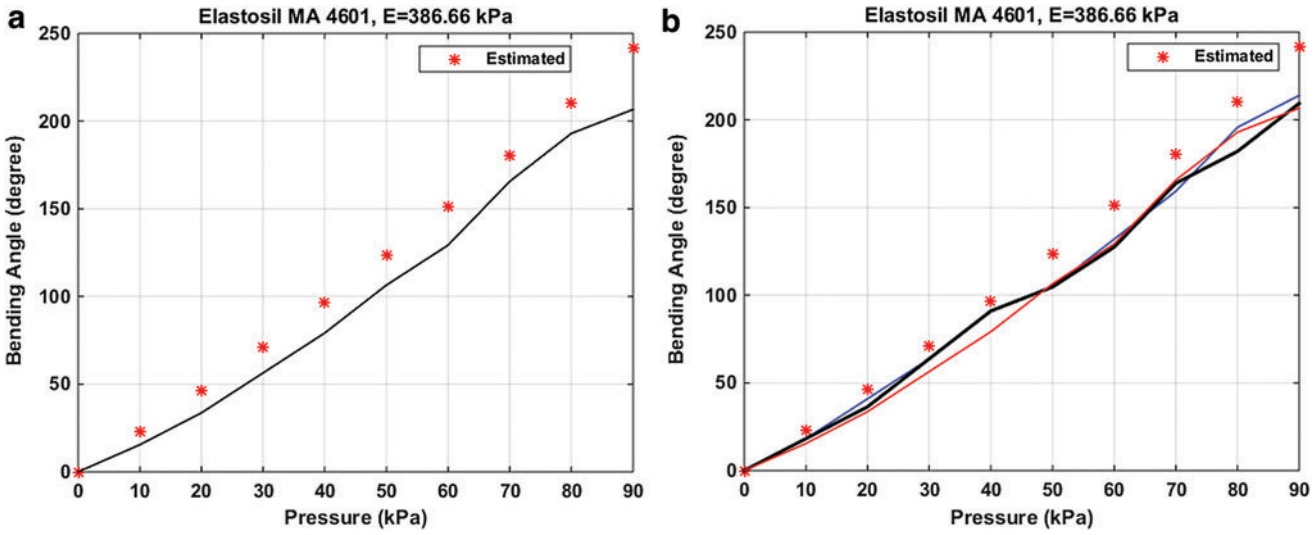

FIG. 6. **(a)** Experimental and estimated results for actuator 1, **(b)** more experimental results showing the validity of the bending angle and blocking force models. The experimental results are shown with the full line. Color images available online at www.liebertpub.com/soro

$$F_B = \eta \frac{\frac{dV}{dt}}{\frac{d\theta}{dt}} \left(\frac{P}{L}\right) = \eta \frac{\dot{V}}{\dot{\theta}} \left(\frac{P}{L}\right) \tag{14}$$

The blocking force is proportional to the pressure provided and inversely proportional to the actuator length that the volume change to the angle change ratio is a constant. This derivation of the blocking force [Equations (10)–(14)] is similar to the derivation for the force output of McKibben actuators.[37,38]

As implementing Equations (13) and (14) can be problematic due to the difficulties associated with analytically expressing the volume change as a function of the bending angle or experimentally measuring this variation, we can use Equation (7) described for the whole actuator to estimate the blocking force F_B. For an experimentally measured radius of curvature R and experimentally identified flexural rigidity EI, the blocking force F_B can be calculated from

$$\frac{\theta}{L} = \frac{1}{R} = \frac{F_B L}{EI}, \; F_B = \theta \; \frac{EI}{L^2} \tag{15}$$

As the actuators considered in this study have a composite structure, composed of an elastomeric material with nonlinearities, rigid ribs, and constraining paper or a bistable thin flexible metal, it is virtually impossible to estimate their effective modulus of elasticity experimentally by using the traditional method of tensile testing. Therefore, we have employed Equation (15) to estimate the effective flexural rigidity (EI) of the actuators with and without the bistable thin metal, if the bending angle and blocking force are known, from

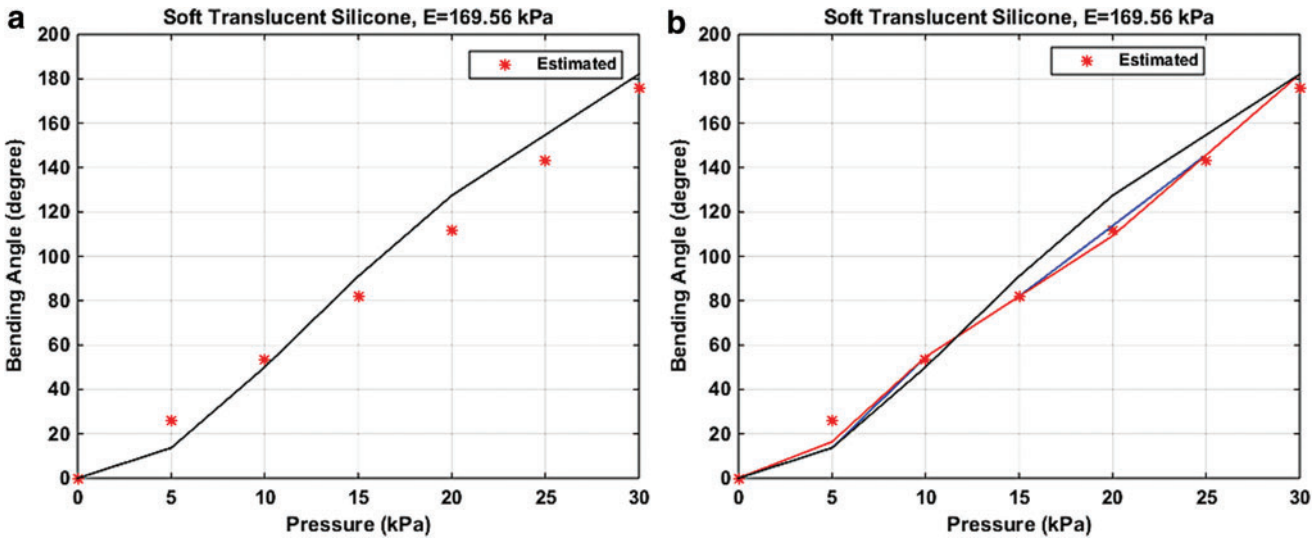

FIG. 7. **(a)** Experimental and estimated results for actuator 2, **(b)** more results showing the validity of the bending angle and blocking force models. The experimental results are shown with the full line. Color images available online at www.liebertpub.com/soro

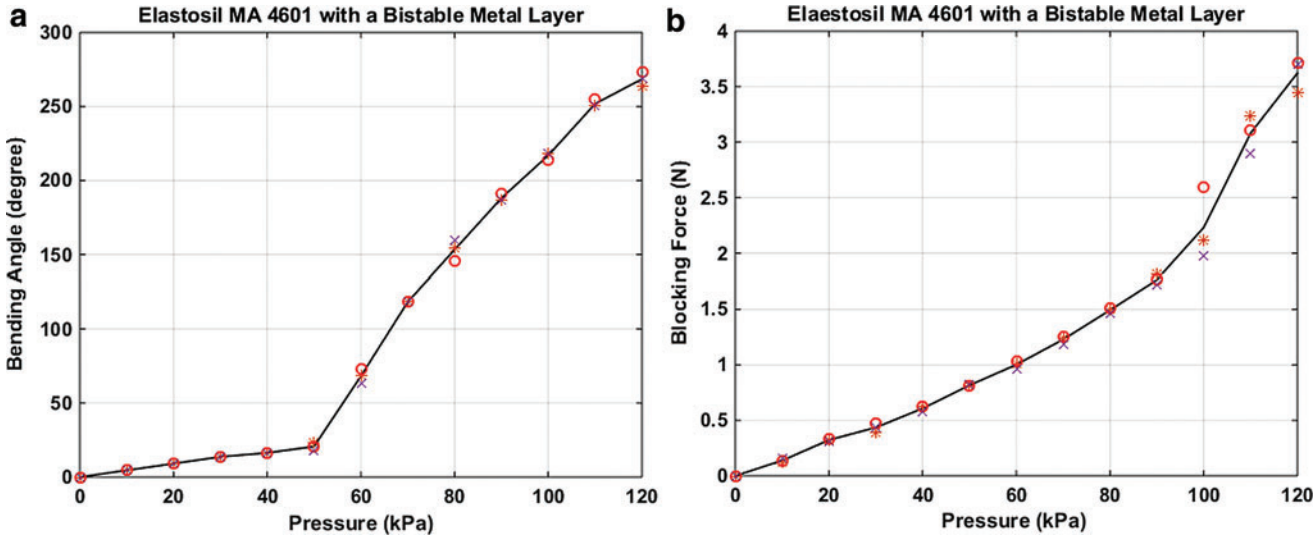

FIG. 8. **(a)** Experimental bending angle versus pressure results, **(b)** experimental blocking force versus pressure results for A1 with a bistable metal layer consisting of a tape measure. The full line shows the average of the three measurements. Color images available online at www.liebertpub.com/soro

$$EI = L^2 \frac{F_B}{\theta} \tag{16}$$

We then calculate the area of moment inertia for the cross-sections in Figure 5, and subsequently calculate the effective modulus elasticity of the actuators, as outlined in the Experimental Validation of Analytical Models section.

Kinematic model

With reference to the bending configurations in Figure 1, the actuator generates a constant curvature with a radius of R and a bending angle of θ. Using the notation in Figure 2, the tip coordinates of the actuator are obtained as

$$\begin{aligned} x &= R\ sin\theta \\ y &= R(1 - cos\theta) \end{aligned} \tag{17}$$

Experimental Validation of Analytical Models

The actuator to be tested was placed in front of a grid paper, as shown in Figure 1, with the pressure incremented at either 5 or 10 kPa, depending on the type of actuator being tested. The deflection was measured through visual inspection of the angle made between the vertical walls of the tip and the base, as described in Figure 2. The bending angle model in Equation (9) requires the geometric parameters, the

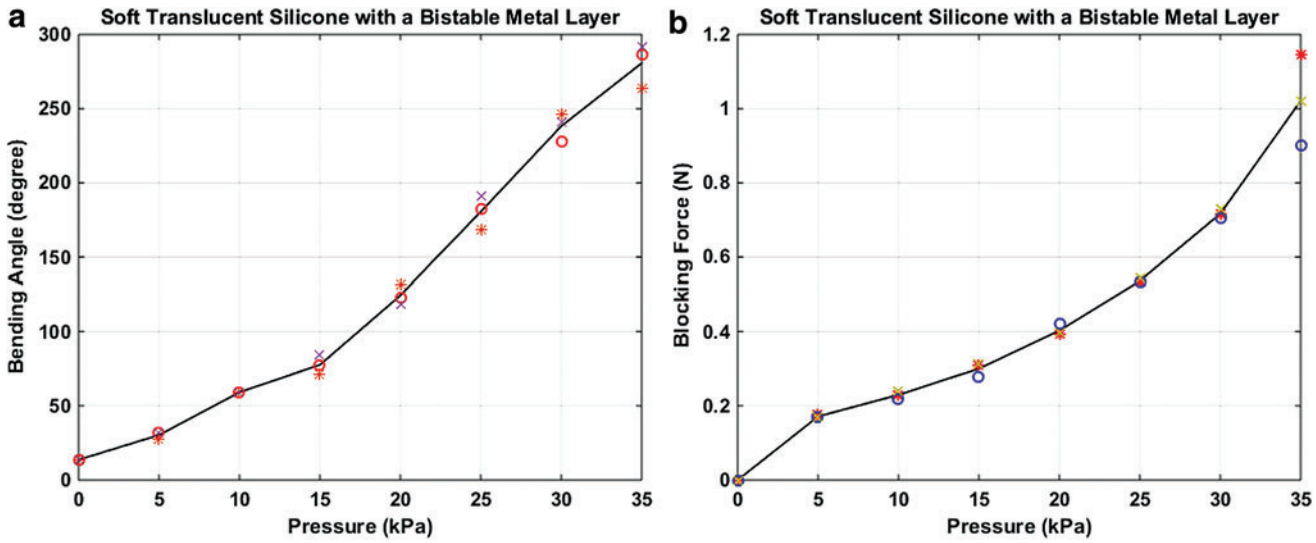

FIG. 9. **(a)** Experimental bending angle versus pressure results, **(b)** experimental blocking force versus pressure results for A2 with a bistable metal layer consisting of a tape measure. The full line shows the average of the three measurements. Color images available online at www.liebertpub.com/soro

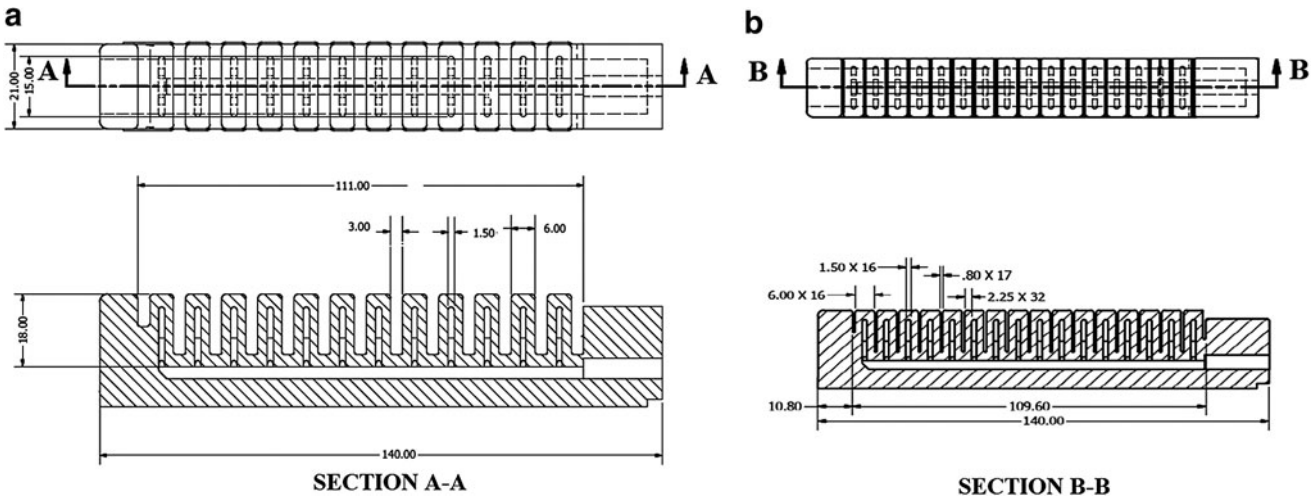

FIG. 10. Geometric dimensions of A3 **(a)** and A1 and A2 **(b)**. It must be noted that the gaps are 3 and 0.8 mm for A3, and A1 and A2, respectively. The other dimensions are the same.

area of moment inertia around the neutral axes, and the effective modulus of elasticity of the actuators. We have employed Equation (16) to determine the flexural rigidity EI and, subsequently, the effective modulus of elasticity of the actuators. It must be noted that measuring the modulus of elasticity of the actuator material experimentally will not be accurate as the actuator structure contains a set of ribs in the middle of each chamber and a layer paper to facilitate the bending of the actuators. We conducted blocking force experiments by using a high-resolution (0.01 g) electronic scale, and the bending angle experiments for two actuators (A1 and A2) made of two different materials. The data in Tables 2 and 3 are used to estimate the effective moduli of elasticity of 386.66 and 169.56 kPa for A1 and A2, respectively, containing a piece of constraining paper layer. It must be noted that the initial deflection in the actuators under zero pressure is deducted from each bending angle measurement. We then used the analytical bending model in Equation (9) to evaluate its validity. The experimental and estimated results are shown in Figures 6a and 7a for A1 and A2, respectively. More experimental results together with the estimated results shown in Figures 6b and 7b indicate the validity of the bending model and the blocking force model, and the methodology followed to estimate the effective modulus of elasticity of the actuators. The proposed model is a gray-box model due to the difficulties associated with incorporating all nonlinear effects in an analytical model, which allows to experimentally identify some parameters of the model using experimental data. This is due to the fact that the modulus of elasticity of the composite structure is totally different than the bulk modulus of elasticity of the elastomeric materials used to construct the chambers. Therefore, the effective modulus of elasticity of the composite actuator is experimentally identified by using the experimental blocking force data. The effective modulus of elasticity was then used in the bending angle model to demonstrate the validity of this model.

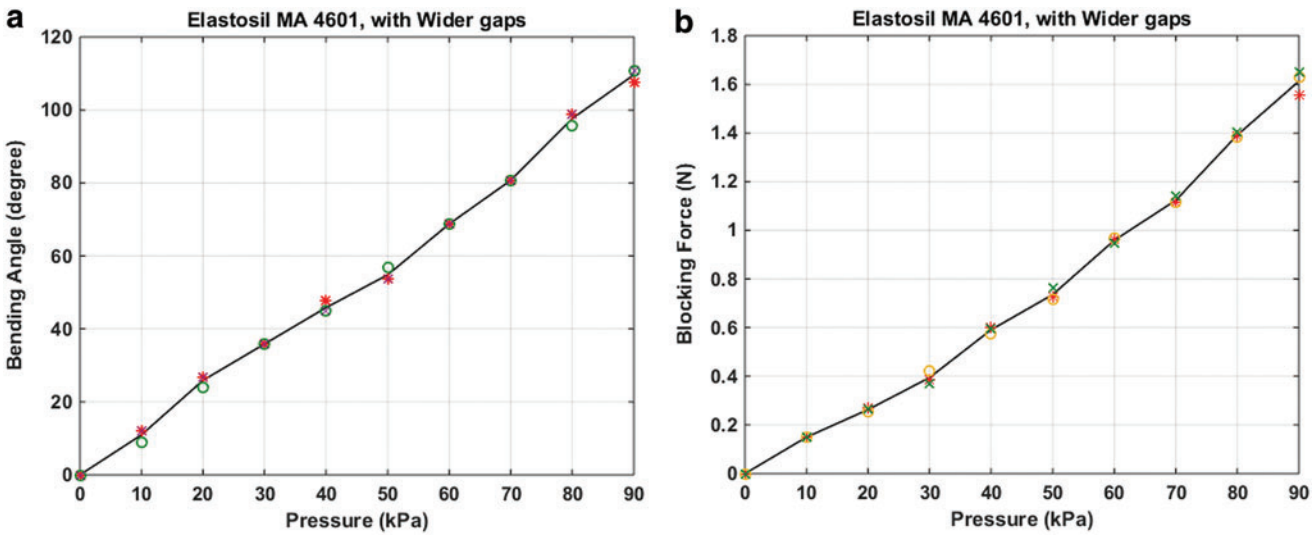

FIG. 11. **(a)** The experimental bending angle versus pressure, and **(b)** blocking force versus input pressure results for A3, the actuator with wider gaps in the between the chambers. Color images available online at www.liebertpub.com/soro

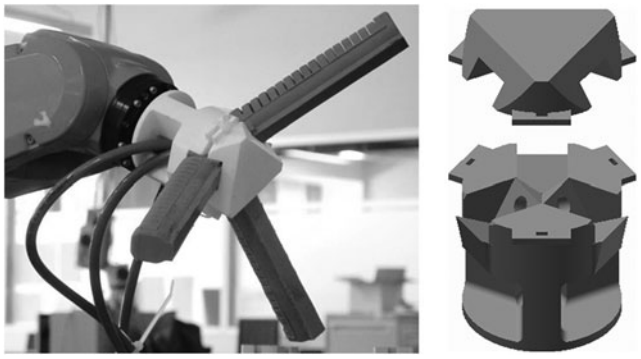

FIG. 12. Soft robotic gripper concept: the gripper (*left*) and housing CAD model (*right*). It must be noted that each finger is in their straight state—thanks to the bistable thin metal layer providing this.

Experimental results with a bistable thin metal

As stated earlier, the soft actuators bend under their own weight. To prevent this, we propose the concept of using a thin bistable metal layer, like a tape measure, to make sure that the actuator keeps its straight configuration in its neutral position, as shown in the top left corner of Figure 1. We fabricated two actuators containing the tape measure, using the silicone materials. We used the same bending angle and blocking force measurement setups. The results are depicted in Figures 8 and 9 for A1 and A2, respectively.

As shown in Figure 8a, the bending angle follows a linear relationship up until 50 kPa, at which point the gradient abruptly changes and becomes much higher, continuing linearly until 120 kPa. The gradient before 50 kPa is $\sim$0.45, and the gradient afterward is 3.65, increasing by a factor of 8. The point at which the gradient of the bending angle rapidly increases is the point at which the bistable thin metal changes between its states of stability. Both data sections before and after 50 kPa slightly flatten out at the end of their run. This can be attributed to the bending moment, being highest when the actuator is not vertical, that causes it to slightly bend under its own weight. With reference to the bending model given by Equation (9), when the effective modulus of elasticity is large enough (>500 kPa), its nonlinear component can be ignored. This follows that Equation (9) indicates a linear behavior, as shown in Figure 8a. Using Equation (16), the effective modulus of elasticity is estimated to be 1.86 MPa and 558.4 kPa for the two states of the thin metal layer for the pressure ranges of 0–50 and 50–120 kPa, respectively.

With reference to Figure 8b, the change in the states of the thin metal layer is not indicated up until 90 kPa in the blocking versus pressure results as the actuator is ideally expected to keep its straight configuration during the force measurements, not allowing significant change in the states of the metal layer. As shown in Figure 8b, the force follows a near-perfect linear relationship up until 90 kPa. After this point, the gradient increases for the range of 90–120 kPa.

As presented in Figure 9b, A2 made of the Soft Translucent silicone has a smaller force output, compared with A1. Therefore, we trimmed (to decrease its width) the bistable thin metal embedded in A2 to decrease its reaction force to bending. The bending angle test for A2 was expected to show the same kind of relationship as A1, but slightly different gradients and points of gradient change. As shown in Figure 9a, the bending angle follows an approximately linear relationship. Although not obvious, at 15 kPa the gradient changes approximately from 4.5 to 10.4 deg/kPa, increasing approximately by a factor of 2. The moduli of elasticity for the initial state and final state are estimated as 218 and 156 kPa, respectively, using Equation (16). This indicates that the bistable thin metal has changed between its states of stability. This transition occurs at the pressure of 15 kPa; whereas for A1, it occurs at the pressure of 50 kPa. The lower critical pressure for A2 can be attributed to two reasons: the softer silicone being used (48 kPa vs. 262 kPa), and a trimmed (smaller width) bistable thin metal that provides less constraining force to overcome.

The ratio of the gradient change between stability states goes from a factor of 8 for A1 to a factor of 2 for A1. This can be attributed to the net force difference between the bending force of the actuators and the opposing force of the bistable thin metal being larger for A1. The bistable thin metal in A1 was not trimmed, making it wider and therefore stiffer. As shown in Figure 9b, the blocking force follows an approximately linear relationship up until 30 kPa. After this point, the gradient slightly increases. As expected, the softer A2 in Figure 9b behaved in a similar manner to that of the stiffer A1 in Figure 8b, with the exception of operating under different pressure ranges. It must be noted that the bending angle

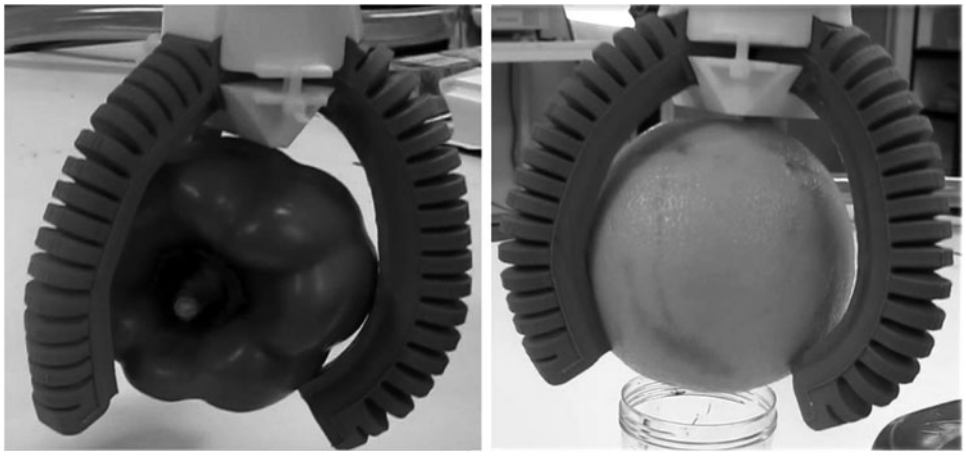

FIG. 13. Actuated gripper holding a capsicum (*left*) and a grapefruit (*right*). (Supplementary Video S1).

versus pressure data in Figure 9a indicate a nonlinear behavior, as predicted by Equation (9) for an actuator with a relatively smaller modulus of elasticity.

Experimental results with an actuator with wider gaps

We conducted bending and blocking force experiments for an actuator made of Elastosil M4601, which we call A3. The geometric dimensions of this actuator and the other two actuators (A1 and A2) are depicted in Figure 10. It must be noted that the gaps in A1 and A2, and A3 are 0.8 and 3.0 mm, respectively. As the actuator length is kept the same for all actuators, the number of chambers for A1 and A2, and A3 are 16 and 12, respectively. The experimental results for A3 are shown in Figure 11. These results are used to estimate the effective modulus elasticity of 359 kPa, which is slightly below the effective modulus of elasticity 387 kPa for A1 made of the same materials. This difference can be due to the fact that the actuators were fabricated and tested in different days when compared with A1, which likely introduced some inevitable measurement and fabrication errors. It must be noted from the results in Figure 11a that the actuator with the larger gaps have generated relatively smaller bending angles. One obvious reason is that the number of pneumatic chambers is decreased from 16 to 12, which will decrease the work input, causing the bending of the actuator, as described by Equation (10).

Applicability: A Soft Robotic Gripper

A housing was built that could hold three of the actuators made of Elastosil M4601 (A1) embedded with the thin metal layer. It was designed to test the feasibility of using the actuators in an industrial gripper. The housing, as shown in Figure 12, was designed to support three actuators that were equidistant from one another (120°) and offset at an angle of −30° from the horizontal. The entire housing was designed to be attached to a robot manipulator, with the housing and actuators acting as the fingers of an effector connected to the tip of the robot manipulator.

The gripper's ability was tested with a number of different objects, including fruit and vegetables, as illustrated in Figure 13. Due to the length and circular profile of the actuators, the gripper was the most effective at holding larger and round objects. However, by decreasing the actuator's length and thus its radius of curvature, smaller objects with irregular shapes can be handled with a multi-finger soft gripper. Figure 13 displays the gripper's ability to handle both spherical (a grapefruit) and nonspherical objects (a capsicum). This is also shown in the accompanying video file (Supplementary Video S1; Supplementary data are available online at www.liebertpub.com/soro). The actuator's compliance allows the gripper to adapt to the objects of varying sizes and shapes without requiring any sensory feedback.

Conclusions and Future Work

We have established an analytical model to predict the bending angle of the slender pneumatic actuators made of discrete pneumatic chambers. The actuators were fabricated from two hyper-elastic silicones. The analytical model has been validated by using the experimental results. Although this is the main achievement of this study, we have proposed a simple method to estimate the effective modulus of elasticity of the actuators made of multi-materials with varying material properties. Another important contribution of this study is to propose a thin flexible metal embedded in the topology of the actuators not only to provide the length-restricting effect needed for bending but also to prevent bending of the actuators under their own weight in their neutral states under zero input pressure.

The future work involves optimizing the mechanical output of the actuator with different cross-sections and materials that they are fabricated from. Other than the input pressure, the modulus of elasticity is the parameter significantly affecting the mechanical output of these actuators [as inferred from Equation (9)]. Taking the modulus elasticity as the important parameter suggests that there is a need for smart materials with a variable modulus of elasticity. Actuators made of such materials can be tailored for various applications as per their variable modulus of elasticity, delivering the proponents of soft robotics in cutting edge applications such as rehabilitation robotics, medical robotics, and assistive devices, for which a soft contact is essential to provide compliance matching between the robotic device and its environment.[10,27,34] The environment is usually an equally soft body, a human being, or an agricultural product, requiring sensitive handling. Soft pneumatic actuators could function effectively in these environments by tolerating inaccuracies in the positioning, shape, and surfaces of such objects.

Acknowledgments

This study was supported by the ARC Centre of Excellence for Electromaterials (ACES) (Grant No. CE140100012). This work is partly supported by the Intelligent Nano-Tera Research Systems Laboratory at University of Wollongong.

Author Disclosure Statement

No competing financial interests exist.

References

1. Rus D, Tolley MT. Design, fabrication and control of soft robots. Nature 2015;521:467–475.
2. Kim S, Laschi C, Trimmer B. Soft robotics: a bioinspired evolution in robotics. Trends Biotechnol 2013;31:287–294.
3. Bauer S, Bauer-Gogonea S, Graz I, Kaltenbrunner M, Keplinger C, Schwoediauer R. A soft future: from robots and sensor skin to energy harvesters. Adv Mater 2014;26:149–162.
4. Alici G. Editorial for Special Issue Mechanics, Control, Design, Conceptualization and Fabrication of Soft Robotic Systems. Available at: www.mdpi.com/journal/robotics/special_issues/soft_robotic (accessed May 20, 2016).
5. Chirikjian GS, Burdick JW. The kinematics of hyper-redundant robot locomotion. IEEE Trans Robot Autom 2005;11:781–793.
6. Kang R, Branson DT, Zheng T, Guglielmino E, Caldwell DG. Design, modeling and control of a pneumatically actuated manipulator inspired by biological continuum structures. Bioinspir Biomim 2013;8:036008.
7. Webster RJ, Jones BA. Design and kinematic modeling of constant curvature continuum robots: a review. Int J Robot Res 2010;29:1661–1683.
8. Pfeifer R, Lungarella M, Iida F. The challenges ahead for bio-inspired soft robotics. Commun ACM 2012;55:76–87.
9. Hauser H, Ijspeert AJ, Fuchslin RM, Pfeifer R, Mass W. Towards a theoretical foundation for morphological

computation with compliant bodies. Biol Cybern 2011;105: 355–370.
10. Mutlu R, Alici G, in het Panhuis M, Spinks GM. 3D printed flexure hinges for soft monolithic prosthetic fingers. Soft Robot 2016;3:120–133.
11. Wakimoto S, Suzumori K, Ogura K. Miniature pneumatic curling rubber actuator generating bidirectional motion with one air-supply tube. Adv Robot 2011;25:1311–1330.
12. Polygerinos P, Wang Z, Overvelde JTB, Galloway KC, Wood RJ, Bertoldi K, *et al*. Modeling of soft fiber-reinforced bending actuators. IEEE Trans Robot 2015;31.
13. Mosadegh B, Polygerinos P, Keplinger C, Wennstedt S, Shepherd RF, Gupta U, *et al.* Pneumatic networks for soft robotics that actuate rapidly. Adv Funct Mater 2014;24: 2163–2170.
14. Ilievski F, Mazzeo AD, Shepherd RF, Chen X, Whitesides GM. Soft robotics for chemists. Angew Chem 2011;123: 1930–1935.
15. Polygerinos P, Lyne S, Wang Z, Nicolini LF, Mosadegh B, Whitesides GM, *et al.* Towards a soft pneumatic glove for hand rehabilitation. In: 2013 IEEE/RSJ International Conference on Intelligent Robots and Systems (IROS). Tokyo, Japan. November 3–7, 2013, pp. 1512–1517.
16. Shepherd RF, Ilievski F, Choi W, Morin SA, Stokes AA, Mazzeo AD, *et al.* Multigait soft robot. Proc Natl Acad Sci U S A 2011;108:20400–20403.
17. Onal CD, Rus D. Autonomous undulatory serpentine locomotion utilizing body dynamics of a fluidic soft robot. Bioinspir Biomim 2013;8:026003.
18. Volder MD, Reynaerts D. Pneumatic and hydraulic microactuators: a review. J Micromech Microeng 2010;20:1–18.
19. Yeo JC, Yap HK, Xi W, Wang Z, Yeow C-H, Lim CT. Flexible and stretchable strain sensing actuator for wearable soft robotic applications. Adv Mater Technol 2016;1. DOI: 10.1002/admt.201600018.
20. Deimel R, Brock O. Novel type of compliant and underactuated robotic hand for dexterous grasping. Int J Robot Res 2016;35:161–185.
21. Shapiro Y, Wolf A, Gabor K. Bi-bellows: pneumatic bending actuator. Sens Actuators A Phys 2011;162:484–494.
22. Gorissen B, Vincentie W, Al-Bender F, Reynaerts D, De Volder M. Modelling and bond-free fabrication of flexible fluidic microactuators with a bending motion. J Micromech Microeng 2015;23:045012.
23. Chang B, Chew A, Naghshineh N, Menon C. A spatial bending fluidic actuator: fabrication and quasi-static characteristics. Smart Mater Struct 2012;21:045008.
24. Sun Y, Song YS, Paik J. Characterization of silicone rubber based soft pneumatic actuators. In: 2013 IEEE/RSJ International Conference on Intelligent Robots and Systems (IROS). Tokyo, Japan. 2013, pp. 4446–4453.
25. Hwang Y, Paydar OH, Candler RN. Pneumatic microfinger with balloon fins for linear motion using 3D printed molds. Sens Actuators A Phys 2015;234:65–71.
26. Yap HK, Ng HY, Yeow C-H. High-force soft printable pneumatics for soft robotic applications. Soft Robot 2016;3: 144–158.
27. Agarwal G, Besuchet N, Audergon B, Paik J. Stretchable materials for robust soft actuators towards assistive wearable devices. Sci Rep 2016;6:34224.
28. Marchese AD, Katzschmann RK, Rus D. A recipe for soft fluidic elastomer robots. Soft Robot 2015;2:7–25.
29. Yang D, Mosadegh B, Ainla A, Lee B, Khashai F, Suo Z, *et al.* Buckling of elastomeric beams enables actuation of soft machines. Adv Mater 2015;27:6323–6327.
30. Alici G. An effective modelling approach to estimate nonlinear bending behaviour of cantilever type conducting polymer actuators. Sens Actuators B Chem 2009;141: 284–292.
31. Moseley P, Manuel Florez J, Sonar HA, Agarwal G, Curtin W, Paik J. Modeling, design, and development of soft pneumatic actuators with finite element method. Adv Eng Mater 2016;18:978–988.
32. Homberg BS, Katzschmann RK, Dogar MR, Rus D. Haptic identification of objects using a modular soft robotic gripper. In: 2015 IEEE/RSJ International Conference on Intelligent Robots and Systems. Germany. 2015, pp. 1698–1705.
33. Bilodeau RA, White EL, Kramer RK. Monolithic fabrication of sensors and actuators in a soft robotic gripper. In: 2015 IEEE/RSJ International Conference on Intelligent Robots and Systems. Germany. 2015, pp. 2324–2329.
34. Mutlu R, Yildiz SK, Alici G, in het Panhuis M, Spinks GM. Mechanical Stiffness Augmentation of a 3D Printed Soft Prosthetic Finger. In: 2016 IEEE/ASME International Conference on Advanced Intelligent Mechatronics. Banff, Canada. 2016, pp. 7–12.
35. Bower DI. An Introduction to Polymer Physics. Cambridge, UK: Cambridge University Press, 2002, pp. 170–172.
36. Timoshenko S. Strength of Materials, Part I, Elementary Theory and Problems, 2nd ed. New York: D. Van Nostrand Company, 1940.
37. Tondu B. Modelling of the McKibben artificial muscle: a review. J Intell Mater Syst Struct 2012;23:225–253.
38. Chou CP, Hannaford B. Measurement and modelling of McKibben pneumatic artificial muscles. IEEE Trans Robot Autom 1996;12:90–102.

Address correspondence to:
Gursel Alici
School of Mechanical, Materials,
Mechatronic and Biomedical Engineering
University of Wollongong
Northfields Avenue
Wollongong 2522
Australia

E-mail: gursel@uow.edu.au